CHEMISTRY OF MATERIALS

pubs.acs.org/cm

Article

Theory-Guided Exploration of the $Sr_2Nb_2O_7$ System for Increased Dielectric and Piezoelectric Properties and Synthesis of Vanadium-Alloyed $Sr_2Nb_2O_7$

Handong Ling, Megha Acharya, Lane W. Martin, and Kristin A. Persson*

Cite This: https://doi.org/10.1021/acs.chemmater.2c00755

Read Online

ACCESS | Metrics & More | Article Recommendations | Supporting Information

ABSTRACT: *Ab initio* methods provide a powerful tool in the search for novel polar materials. In particular, there has been a surge to identify lead-free piezoelectric materials to replace $PbZr_{0.52}Ti_{0.48}O_3$. This study examines a computational strategy to identify increased piezoelectric and dielectric responses of alloy systems based on the linear interpolation of force constants, Born effective charges, and internal strain tensors from their end-point compounds. We choose the ferroelectric layered perovskite $Sr_2Nb_2O_7$ as a parent structure and employ this alloying strategy for 19 potential cation substitutions, targeting thermodynamically metastable alloys with high piezoelectric response. From this screening, we identify $Sr_2Nb_{2-2x}V_{2x}O_7$ as a promising polar system. We conduct large-unit-cell calculations of $Sr_2Nb_{2-2x}V_{2x}O_7$ at x = 0.0625, 0.125 for multiple cation orderings and find a significant 184% enhanced piezoelectric response. The solid solution system is synthesized as single-crystalline thin-film heterostructures using pulsed-laser deposition, and an enhanced dielectric response is observed at x = 0.05 and at x = 0.1. We present the $Sr_2Nb_{2-2x}V_{2x}O_7$ alloy system designed through high-throughput computational screening methods with a large calculated piezoelectric response and experimentally verified increased dielectric response. Our methodology is provided as a high-throughput screening tool for novel materials with enhanced polarizability and alloy systems with potential morphotropic phase boundaries.

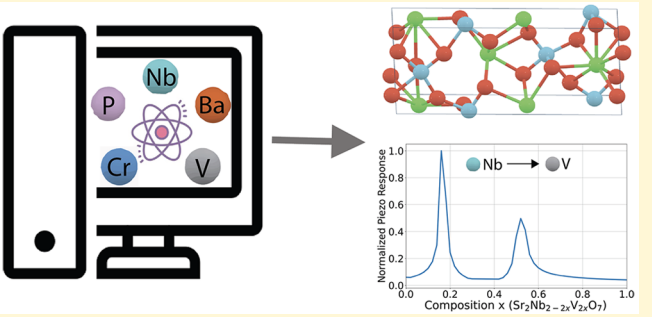

INTRODUCTION

Near the morphotrophic phase boundary (MPB) compositions, ceramics may exhibit anomalously large piezoelectric and dielectric properties arising from the flattening of the energy landscape between polarization states.[1] This materials design paradigm has delivered high-performance, technologically successful materials such as $PbZr_{0.52}Ti_{0.48}O_3$ (PZT), which displays both strong piezoelectric as well as dielectric behavior. However, in light of the increasing global restrictions on lead,[2] there is a strong driving force to identify lead-free piezoelectric replacements. The current, ubiquitous use of PZT in devices is estimated to contribute up to 25% of the total lead in our future electronic waste streams.[2] In addition to environmental concerns, PZT exhibits a Curie temperature of approximately 400 °C, limiting its use in high-temperature devices.[3]

The majority of current lead-free MPB research is focused on perovskite-structured materials, namely $K_xNa_{1-x}NbO_3$ (KNN), $BiFeO_3$ (BFO), and $Bi_{0.5}Na_{0.5}TiO_3$ (BNT) alloys.[4] These systems all exhibit enhanced polarizability associated with a rhombohedral-to-tetragonal phase transition induced by changes in chemical composition. As a result, their piezoelectric and dielectric properties present solutions for specific applications such as energy harvesters, high-frequency transducers, actuators, and capacitors. However, issues with processing and temperature stability limit these alternative perovskites from providing a generic replacement for PZT.[5] Computational explorations of the perovskite chemical space suggest that studies of structures outside of the traditional perovskite family may be required to provide a successful lead-free competitor to PZT.[6,7] In addition, other structural families, e.g. tungsten bronze, have garnered attention as high-temperature solutions.[8]

In this context, computation can serve as a valuable additional resource in the search for possible prototype structures, particularly outside of traditional perovskites which exhibit a rhombohedral to tetragonal phase transition. The Materials Project has developed and benchmarked workflows for the calculation of the full piezoelectric as well as the dielectric tensor.[9,10] To date, these workflows have produced piezoelectric and dielectric tensors for over 3400 and 7100 crystalline materials, respectively. However, these high-

Received: March 14, 2022
Revised: August 3, 2022

throughput density functional theory (DFT) calculations are restricted to bulk, ordered crystals of limited unit-cell size. Strong piezoelectrics, meanwhile, are typically dominated by solid solution disordered alloys, such as PZT, KNN, La or Sm doped BFO, and BNT close to MPBs. In these alloy systems, the free energy landscape flattens near the solid solution phase boundary, allowing for easy switching of the polarization direction and in turn increased piezoelectric and dielectric response.[1] Therefore, a successful computational search for piezoelectric materials will require the modeling of solid solution alloys near MPBs. However, *ab initio* screening methods have historically focused on ordered materials, as the effects of off-stoichiometry and random ionic disorder can be difficult to capture within a limited-size, periodic supercell.

MPBs are characterized by the softening of phonon modes which indicate the emerging preference of the structure to adopt a new structural symmetry.[11,12] Therefore, calculating the lattice dynamic properties as an alloy changes in composition is essential to determining the presence of potential MPBs and enhanced piezoelectric response near the phase boundary. Lattice dynamic properties of solid solutions have been previously modeled by averaging the properties of special quasi-random structures (SQS), generating transferable force constants, or self-consistent phonon approaches.[13−17] Transferable force constants have been used to determine vibrational entropies of mixing for aluminum−transition-metal alloys.[14] More recently, self-consistent calculations of phonon modes have been used to generate force constants suitable for molecular dynamics in MoS_2 monolayers.[16] These methods, however, can be computationally expensive for high-throughput searches, limiting the possibility of exploring large solid solution alloy systems.

In this paper, we develop a computational methodology to extensively explore candidate piezoelectric alloy systems for increased polar response by using a Vegard's law like linear approximation to model the Born effective charges, internal stain tensor components, and force constants of an alloy from its compositional end points. We first demonstrate the efficacy of this approach on PZT to model the softening phonon modes around the MPB and behavior of polar properties associated with the phase transition. We then choose a layered perovskite structure, $Sr_2Nb_2O_7$, and explore the possibility of increased polar response as a function of alloying with a high-throughput framework. Recent work,[18] which focused on identifying defect-tolerant materials and structural classes which retain much of their piezoelectric response with respect to disorder, identified $Sr_2Nb_2O_7$ as a promising parent compound. The layered perovskite $Sr_2Nb_2O_7$ has been synthesized previously and is a known ferroelectric material with a Curie temperature above 1200 °C.[19,20] In addition, substitutional alloy systems of $Sr_2Nb_2O_7$ with barium, vanadium, and tantalum have also been synthesized, demonstrating the ability of this system to support stable, disordered solid solutions.[21−23] Focusing on the lattice dynamic properties of this system, we explore suitable substitutions on both the Sr and Nb cation sites for improved piezoeletric and dielectric responses near regions of softened phonon modes. We use the Vegard's-law-like linear approximation to model the alloy space between the compositional end points, which allows us to tractably explore alloy systems of the parent $Sr_2Nb_2O_7$ material. Promising alloys are assessed for thermodynamic stability, and large-scale DFT calculations are employed on the best-performing alloy system, $Sr_2Nb_{2-2x}V_{2x}O_7$, in order to validate the linear interpolation approach. Following the recommendations obtained by DFT calculations for enhanced polar behavior, the system is synthesized through pulsed-laser deposition and increased dielectric properties are found. Along with this general methodology for systematically exploring disorder-tolerant[18] piezoelectric alloy systems, we identify $Sr_2Nb_{2-2x}V_{2x}O_7$ as a promising system with confirmed increased dielectric and predicted increased piezoelectric properties.

PROCEDURES

Computational Procedures. The candidate substitutional alloy systems we consider in the study are $Sr_{2-2x}A_{2x}Nb_2O_7$ and $Sr_2Nb_{2-2x}B_{2x}O_7$, where A = {Ca, Ba} and B = {As, Au, Bi, Cr, Ir, Mo, N, Os, P, Pt, Re, Rh, Ru, Sb, Ta, V, W}. This includes all nonradioactive elements which were deemed as possible isovalent substitutions on the cation sites: i.e., they exhibit the same oxidation state and occupy the same coordination environment as in the layered perovskite structured $Sr_2Nb_2O_7$. The Born effective charges, internal strain tensors, and force constants of structures at the end points of these alloy systems are calculated using density functional perturbation theory (DFPT),[9,24−26] utilizing the Vienna ab initio simulation package (VASP)[27,28] within the PBE generalized gradient approximation (GGA+U).[29] Full calculations on U values, spin polarization, and pseudopotential choices can be found in Additional Computational Procedures in the Supporting Information. An initial structural relaxation is conducted at an energy cutoff of 700 eV. Then an energy cutoff for the plane waves is set at 1000 eV with a k-point density of approximately 2000 per reciprocal atom (pra) for the piezoeletric DFPT calculations.[30] The Born effective charges and internal strain tensors are atomic site properties calculated for all atoms in the 22-atom orthorhombic unit cell, while the force constants are calculated for each atom pair in the unit cell. Subsequently, the piezoelectric tensor in this study is calculated as

$$e_{\alpha j} = \overline{e}_{j\alpha} + \Omega_0^{-1} Z_{m\alpha} (K^{-1})_{mn} \Lambda_{nj} \quad (1)$$

where e is the total piezoelectric tensor, $\overline{e}$ is the electronic or clamped ion contribution to the piezoelectric tensor, and the remaining terms represent the relaxed ion contribution. The relaxed ion contribution consists of the unit cell volume, Ω_0, the Born effective charge Z, the force constant matrix K, and the internal strain tensor, Λ.[30] Similarly, the dielectric tensor is calculated as

$$\chi_{\alpha\beta} = \overline{\chi}_{m\alpha} + \Omega_0^{-1} Z_{m\alpha} (K^{-1})_{mn} Z_{n\beta} \quad (2)$$

We note that the dielectric and piezoelectric tensors are often correlated due to the inclusion of the Born effective charges and force constants.[3,30] We neglect the contribution of the electronic term in the piezoelectric calculation, $\overline{e}$, in this study as it generally does not contribute significantly to the total piezoelectric tensor for the materials currently computed in the Materials Project database.[18] Once the piezoelectric properties for the fully substituted alloys are computed, we approximate the piezoelectric tensor for the intermediate compositions of the substitutional alloy systems by employing a Vegard's-law-like linear approximation for the Born effective charges, internal stain tensors, and force constants of the alloy. The force constants and associated phonon spectra of alloy systems can be particularly expensive to obtain computationally. Korman et al. demonstrated, however, that for long wavelengths and low frequencies relevant to the piezoelectric response, the phonon spectra of high-entropy alloys may be reasonably reproduced by averaging force constants from end-point compositions.[31] All piezoelectric responses reported in the study are the largest absolute singular value of the total piezoelectric tensor.

The candidate $Sr_{2-2x}A_{2x}Nb_2O_7$ and $Sr_2Nb_{2-2x}B_{2x}O_7$ alloys need to exhibit a stable solid solution such that force constants, Born effective charges, and internal strain properties vary gradually with composition and to allow for the possibility of a MPB to form. Hence, alloy

https://doi.org/10.1021/acs.chemmater.2c00755
Chem. Mater. XXXX, XXX, XXX−XXX

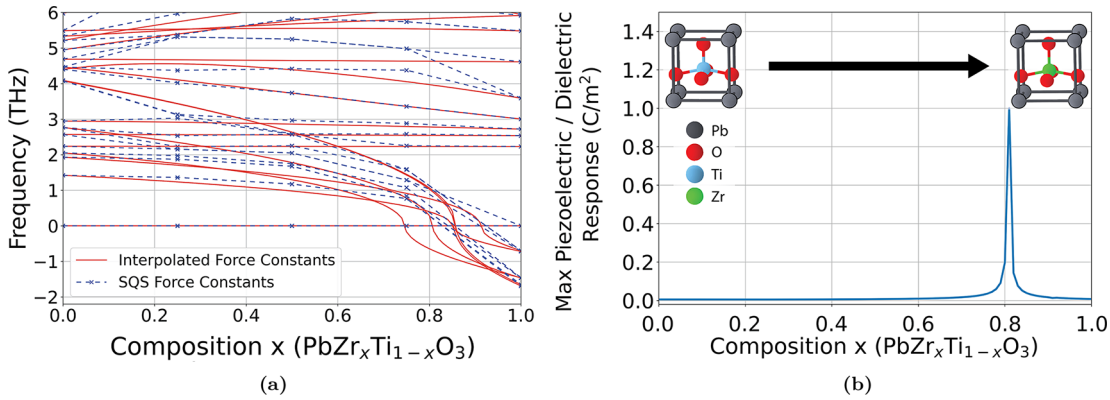

Figure 1. (a) The normalized largest singular value of the piezoelectric and dielectric tensor calculated from the linearly interpolated force constants, Born effective charges, and internal strain tensors of the end-point compositions generated through DFT.(b) The associated γ-point phonon frequencies of the PZT system plotted from a linear interpolation of force constants in red compared against those calculated from averages of SQSs at varying compositions in blue.

systems are further evaluated for thermodynamic metastability. All possible cation site orderings within a 44-atom unit cell across the selected composition space are enumerated, and energies of the relaxed structures are calculated using DFT with an energy cutoff of 700 eV and 1000 k-points per reciprocal atom. Metastability for each ordering in these systems is approximated as 0.1 eV per atom above the hull,[36] which captures approximately 80% of experimentally observed metastable oxides.[32] In addition to metastability, a stable solid solution criterion is set at an energy range of 0.025 eV per atom (approximately equal to k_BT at room temperature) between the lowest and highest energy orderings at a given composition.[32]

Finally, for the most promising candidate system $Sr_2Nb_{2-2x}V_{2x}O_7$, which demonstrates a large predicted increase of its piezoelectric and dielectric properties, we perform 88-atom supercell calculations to more accurately model the polar response of the disordered system. The calculations of the $Sr_2Nb_{2-2x}V_{2x}O_7$ supercell structure use an energy cutoff of 700 eV and an electronic energy convergence of 10^{-6} eV. Structures are relaxed to a force of less than 0.02 eV/Å, and then the Born effective charges, internal strain tensor, and force constant matrices are calculated. The Born effective charges are obtained through DFPT. The internal strain tensor is fitted to forces from 20 strains between −0.01 and 0.01 for each of the Cartesian and shear strains. Analyses of the force constants and dynamical matrix are performed with DFT and the Phonopy package.[33] The Born effective charges, internal strain tensors, and force constants are calculated for multiple special quasirandom structures (SQS), obtained through an alloy theoretic automated toolkit (ATAT), to ensure the response is not dependent on a specific cation ordering.[34] These SQSs are chosen such that the generated unit cells contain cluster vectors which most closely match those of truly random alloys so as to construct solid solutions in a mathematically rigorous manner.[34] To compute the dielectric tensors, the electronic portion is calculated through DFPT. The ionic portions of the tensors are calculated from the Born effective charges and force constants as specified by Wu et al.[30]

Piezoelectric tensors and force constants are also calculated for $PbZr_xTi_{1-x}O_3$ compositions (x = 0, 0.25, 0.5, 0.75, 1) through DFPT, with the same parameters as for the layered perovskite systems. For each composition, 5 20-atom SQSs are obtained through the ATAT package. The Born effective charges, internal strain tensors, and force constants of each SQS at a given composition are then averaged to more accurately capture the properties of the solid solution.[13,34] This procedure is aimed at comparing the force constants generated from a a linear interpolation of end-point site properties against those generated from multiple SQSs at specific compositions for a well-studied system. In this study, the piezoelectric properties of multiple SQSs are averaged by taking the mean of the Born effective charges, internal strain tensors, and force constants for each atomic site among all orderings and then subsequently calculating the piezoelectric tensor for these average properties. Symmetries are taken into account by counting each symmetry-equivalent transformation of each SQS as a distinct ordering in the mean.

Experimental Procedures. *Growth of Thin-Film Heterostructures.* The thin-film heterostructures with compositions $Sr_2Nb_{2-2x}V_{2x}O_7$ (x = 0, 0.05, 0.1) were deposited using pulsed-laser deposition in an on-axis geometry with a KrF excimer laser (248 nm, LPX 300, Coherent) and a target to substrate distance of 55 mm. Films with a range of thicknesses (50−300 nm) were grown on $SrTiO_3$ (110) substrates over a range of growth conditions using ceramic targets with compositions $Sr_2Nb_2O_7$ and $Sr_2V_2O_7$. The solid solution compositions (i.e., $Sr_2Nb_{2-2x}V_{2x}O_7$, x = 0.05, 0.1) were first synthesized utilizing alternate ablation from the two parent targets (i.e., $Sr_2Nb_2O_7$ and $Sr_2V_2O_7$) via sub-unit-cell-level mixing using a programmable target rotator (Neocera, LLC) synced with the excimer laser. Next, individual targets with compositions $Sr_2Nb_{2-2x}V_{2x}O_7$ (x = 0.05, 0.1) were used for synthesizing the final heterostructures. The best results were obtained for the growths performed at a heater temperature of 750 °C (for x = 0) and 600 °C (for x = 0.05, 0.1) with a laser fluence of 3.75 J/cm^2 and a laser repetition rate of 10 Hz at a dynamic oxygen partial pressure of 100 mTorr. In all cases, 30−45 nm thick $La_{0.7}Sr_{0.3}MnO_3$ films were used as the conductive oxides for the bottom and the top electrodes in the heterostructures. The $La_{0.7}Sr_{0.3}MnO_3$ films were grown at a heater temperature of 750 °C with a laser fluence of 2 J/cm^2 at a laser repetition frequency of 2 Hz and a dynamic oxygen partial pressure of 100 mTorr. All of the heterostructures were cooled to room temperature from the temperature of growth at a rate of 10 °C/min in a static oxygen pressure of 700 Torr.

Structural Characterization Using X-ray Diffraction. X-ray diffraction studies were performed using a high-resolution X-ray diffractometer (Panalytical, X'Pert MRD) with a fixed slit of 1/2° in the incident beam optics (Cu Kα radiation with λ = 1.54 Å) and a receiving slit of 0.275 mm in the diffracted beam optics (PIXcel3D-Medipix3 detector). The crystal structures of the synthesized thin-film heterostructures were determined in the direction perpendicular to the plane of the substrate using θ−2θ line scans.

Dielectric Characterization. The dielectric properties for the heterostructures with compositions $Sr_2Nb_{2-2x}V_{2x}O_7$ (x = 0, 0.05, 0.1) were measured using an E4990A Impedance Analyzer (Keysight Technologies) with an applied DC electric field strength from −1000 to 1000 kV/cm at a frequency of 10 kHz.

RESULTS AND DISCUSSION

Linear Approximation to Predict Phonon Softening in $PbZr_xTi_{1-x}O_3$. The primary work of our methodology is to accurately determine the properties of intermediate alloy compositions through interpolation from the properties of their end-point compounds. Therefore, we first demonstrate

https://doi.org/10.1021/acs.chemmater.2c00755
Chem. Mater. XXXX, XXX, XXX−XXX

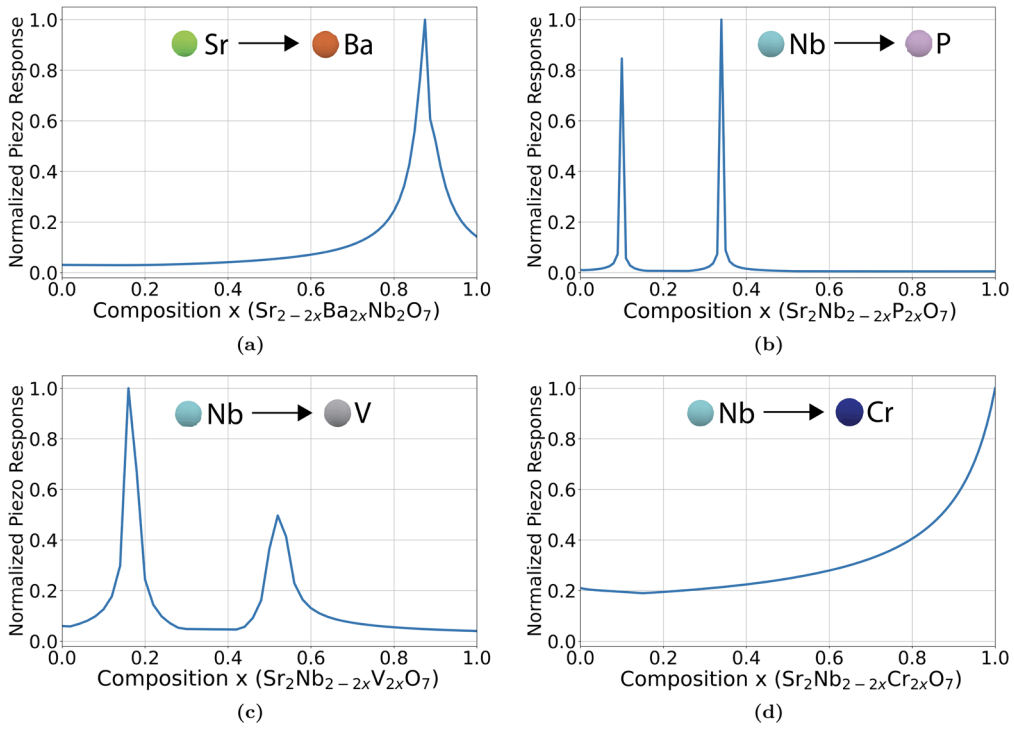

Figure 2. Normalized largest singular values of the piezoelectric and dielectric tensors for alloy systems of the $Sr_2Nb_2O_7$ system as approximated from a linear interpolation of properties from $Sr_{2-2x}A_{2x}Nb_2O_7$ and $Sr_2Nb_{2-2x}B_{2x}O_7$ alloy end points. The four alloys shown all contain peaks in the approximated piezoelectric response, which indicates the potential for enhancement in response as phonon modes soften during alloying.

that linearly interpolating force constants, Born effective charges, and internal strain tensors between the end-points composition in the well-studied tetragonal *P4mm* PZT phase yield reasonable predictions of trends in the dynamic and piezoelectric properties compared to more comprehensive DFT calculations. In Figure 1a, we plot (in red) the γ-point phonon spectra generated from linearly interpolating the DFPT force constants from end point compounds. These force constants are used to produce the piezoelectric response in Figure 1b. The primary factor contributing to the peak in our approximation of the piezoelectric response shown in Figure 1b is the softening of lattice dynamic properties also observed experimentally in PZT.[12] In order to examine how well linearly interpolated force constants capture lattice dynamic properties at intermediate compositions, we compare to the spectra calculated from averaging multiple SQS force constants. The force constants are calculated for five $PbZr_xTi_{1-x}O_3$ compositions (x = 0, 0.25, 0.5, 0.75, 1). With increasing zirconium content, the phonon modes of the PZT system derived from average SQS results soften and become unstable at approximately x = 0.85. Using the linearly interpolated end-point force constants, we find that the overall trend of phonon modes softening is well described, noting that dynamic instability is predicted at a slightly lower zirconium content (x = 0.75). More generally, the phonon frequencies show good agreement between the linear interpolation of force constants and averaging of SQS force constants as a function of composition.

The calculated softening of phonon modes is associated with an increase in polarizability leading to the peak in approximated piezoelectric and dielectric response in Figure 1. We note that the approximated dielectric and piezoelectric responses in Figure 1b are identical, as both are discontinuous with respect to instabilities in the force constant matrix. Experiments show a similarly large enhancement of piezoelectric properties in PZT at 52% zirconium,[35] significantly lower than the onset of dynamical instability as predicted by both computational methods. However, we note thatit is common for first-order phase transformations to occur before the complete destabilization of the lattice, which is indicative of a second-order transition. Hence, phonon instabilities can be used as descriptor of possible phase transitions. We summarize that the experimentally observed presence of a PZT MPB, a large increase in the piezoelectric and dielectric properties, and softening of the phonon modes associated with the B-site atom distorting the oxygen cage are all qualitatively captured by the linearly interpolated force constant methodology.[12] While the softening phonon modes in an alloy do not necessitate the presence of an MPB, they can regardless lead to a predicated enhancement of polar properties. In this PZT system, the approximated phonon instabilities are indeed associated with an MPB, which demonstrates the potential for this approximation to act as a high-throughput descriptor for MPBs in alloy systems.

Exploration of $Sr_2Nb_2O_7$ Alloy Systems. Subsequently, we utilize linearly interpolated force constants, Born effective charges, and internal strain tensors to approximate the piezoelectric response for all candidate alloys originating from the parent $Sr_2Nb_2O_7$ compound. These alloy systems include site substitutions of 2 elements on the strontium site and 17 elements on the niobium site, as given in the Computational Procedures. The approximated piezoelectric response is examined for enhancement near compositions with softened phonon modes in each of these substitutional systems. We highlight alloy systems with barium substitution on the *A* site and phosphorus, vanadium, and chromium substitution on the *B* site as promising potential polar systems based on their approximated response at intermediate

https://doi.org/10.1021/acs.chemmater.2c00755
Chem. Mater. XXXX, XXX, XXX−XXX

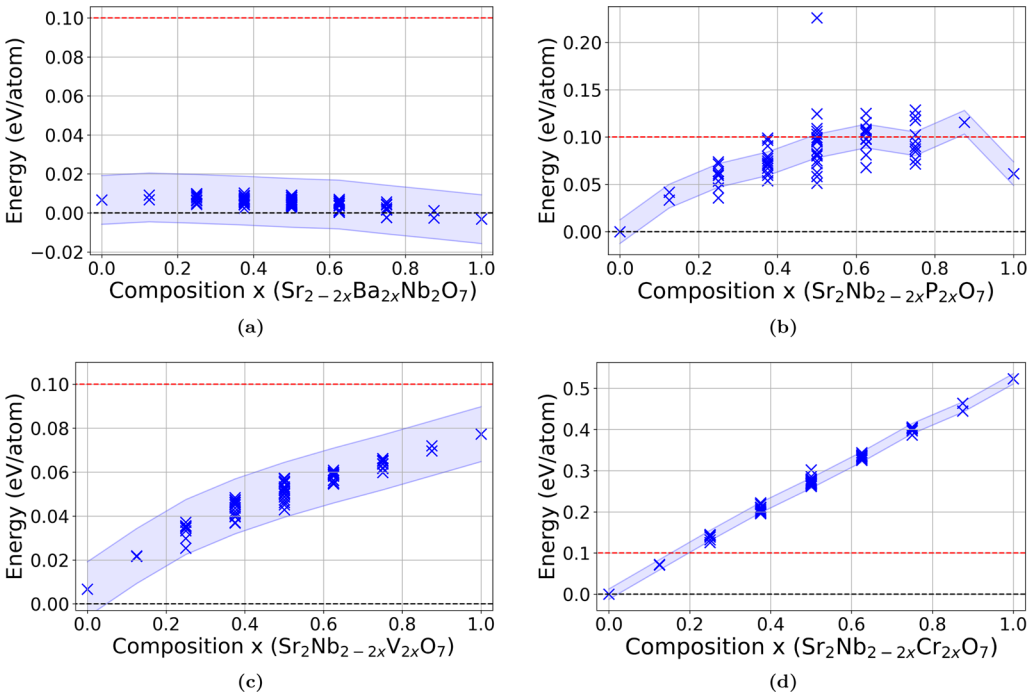

Figure 3. Computed energies above the hull of all orderings within 44-atom unit cells of four promising alloy systems calculated in order to determine guidelines for metastability and solid solution stability. The blue crosses represent structures in the parent $Cmc2_1$ space groups. Criteria for a metastable solid solution are that structures at a given composition must be below 0.01 eV/atom above the hull indicated by the red line and within 0.025 eV/atom of each other indicated by the blue shading. The convex hull, as taken from compounds present in the Materials Project, is shown at an energy of 0 eV/atom as a black line.

compositions shown in Figure 2. In these alloy systems, a dramatic increase in the piezoelectric response is associated with phonon modes softening as a function of alloy composition. All other systems, including those which also demonstrate a discontinuous increase in piezoelectric response but present a large number of unstable phonon modes, are shown in Figure 1 in the Supporting Information.

We next take into consideration the thermodynamic stability of alloys from the parent $Sr_2Nb_2O_7$ system. We plot the energy above the hull for all possible cation orderings within a 44-atom unit cell of each alloy as a function of composition in Figure 3. An energy above the hull lower than 0.1 eV per atom suggests metastable ordering, and a maximum energy range of less than 0.025 eV per atom at a given composition implies a metastable solid solution as described in Procedures.[32] From Figure 3d, we find that many orderings of the $Sr_2Nb_{2-2x}Cr_{2x}O_7$ alloy system present steep increases of thermodynamic instability as a function of chromium content (note the considerably larger vertical axis scale), which likely indicates that any attempted alloy at compositions close to the predicted increase in piezoelectric response (see Figure 2d) will decompose during synthesis. Therefore, we exclude this system from further investigation. Figure 3b suggests that compositions in the $Sr_2Nb_{2-2x}P_{2x}O_7$ alloy systems are unlikely to form solid solutions, especially in the intermediate alloy range $0.2 < x < 0.8$. The maximum piezoelectric response for the $Sr_2Nb_{2-2x}P_{2x}O_7$ system lies at around $x = 0.1$, suggesting that niobium-rich versions of this alloy may present viable candidates to form solid solutions with enhanced properties. In particular, from Figure 3a,c we note that $Sr_{2-2x}Ba_{2x}Nb_2O_7$ and $Sr_2Nb_{2-2x}V_{2x}O_7$ alloys are metastable throughout the composition range and likely amenable to be present as solid solutions. For the purposes of this study, we will consider the $Sr_2Nb_{2-2x}V_{2x}O_7$ system for further study, as the barium-substituted compound has been synthesized and was shown to form a $Ba_5Nb_4O_{15}$ secondary phase.[12]

Focusing on the $Sr_2Nb_{2-2x}V_{2x}O_7$ system, we further explore the approximation of large piezoelectric response by constructing an 88-atom system and computing the piezoelectric and dielectric response at select compositions.[33] The piezoelectric response generated from linear approximations of end-point properties (Figure 2c), as well as the thermodynamic stability window (Figure 3c), indicates that compositions below 20% vanadium composition are likely to produce stable materials in the layered perovskite structure with large piezoelectric properties. For these reasons, we choose compositions of $x = 0.0625$, 0.125 to conduct these large-scale DFT calculations.

Figure 4 shows the results of DFT calculations of the polar properties for 88-atom unit cell $Sr_2Nb_{2-2x}V_{2x}O_7$ alloys. In order to demonstrate the effect of specific orderings on the piezoelectric and dielectric properties, we calculate the tensors for both unique orderings in the unit cell at the $x = 0.0625$ composition and three distinct SQSs at the $x = 0.125$ composition. The dielectric response in Figure 4 is shown in red for [001], as this is the out-of-plane direction for the synthesized thin film for which the dielectric constant is measured. There is a limited increase in dielectric constant for one of the orderings at $x = 0.0625$, but otherwise no dielectric enhancement is predicted. The piezoelectric response of each unique ordering is shown in Figure 4 as a blue ×, and we find an enhanced piezoelectric response from $Sr_2Nb_2O_7$ for all vanadium alloys. This enhancement is primarily found in the d_{33} and d_{14} components of the piezoelectric tensor. In order to reproduce the properties of the solid solution, we also average the values of the Born effective charges, internal strain tensors,

https://doi.org/10.1021/acs.chemmater.2c00755
Chem. Mater. XXXX, XXX, XXX−XXX

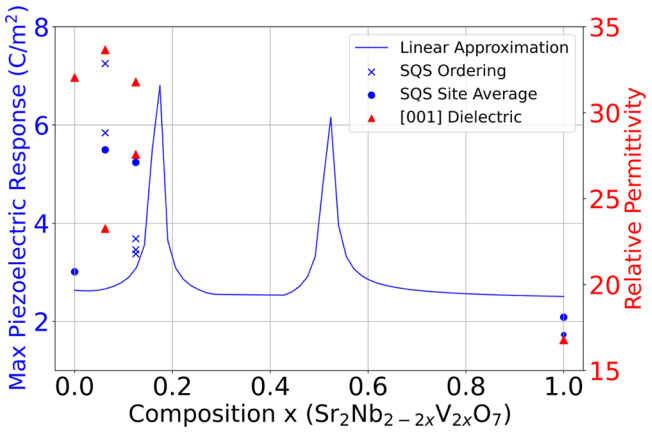

Figure 4. Largest singular values of the piezoelectric tensor of 88-atom unit cells of the $Sr_2Nb_{2-2x}V_{2x}O_7$ system. Three SQS orderings generated from ATAT at $x = 0.125$ and both unique orderings at $x = 0.0625$ are shown. The piezoelectric responses generated from an average of the force constants, Born effective charges, and internal strain tensors of all orderings at each composition are shown as solid circles. The approximation generated from a Vegard's law interpolation of properties from $Sr_2Nb_2O_7$ and $Sr_2V_2O_7$ is shown in the background. Dielectric constants in [001] for individual SQS orderings of the structure are shown in red.

and force constants from these three individual SQS orderings and all symmetrically equivalent sites as defined in Procedures before calculating the piezoelectric tensor. These results are shown separately from the direct DFT calculations in Figure 4 as circles. In general, we observe that the results of the large-scale DFT calculations are consistent with results from the linear approximation, although they are shifted (by approximately $x = 0.05-0.1$) to slightly lower vanadium concentrations. At a composition of $x = 0.0625$ we find that the individual orderings produce a 2-fold increase in the piezoelectric response. Similarly the piezoelectric response generated from an average of properties from these two orderings produces a response of 5.49 C/m^2. At the $x = 0.125$ composition, there is a modest increase in the piezoelectric response for all orderings. However, the piezoelectric response calculated from an average of Born effective charges, internal strain tensors, and force constants of three SQSs at $x = 0.125$ demonstrates a piezoelectric response which is 174% of that of the $Sr_2Nb_2O_7$ end point. The enhancement in piezoelectric response was found to be most strongly associated with the force constants and internal strain tensors of the Nb/V cation site and corresponding oxygen cage. In addition, we report that there are no dynamic instabilities (imaginary phonon mode frequencies) at the γ point for the calculated alloys when the force constants are averaged across their SQS orderings.

Experimental Results. Motivated by the DFT predictions, we synthesized and characterized 100−300 nm thick single-crystalline (001)-oriented $Sr_2Nb_{2-2x}V_{2x}O_7$ (x = 0, 0.05, 0.1) films on (110)-oriented $SrTiO_3$ substrates. $La_{0.7}Sr_{0.3}MnO_3$ films that were 30−45 nm thick were used as bottom and top electrodes. All of the synthesized heterostructures were single crystalline, as shown in the X-ray diffraction ($\theta-2\theta$) line scans in Figure 5a. The parent compound $Sr_2Nb_2O_7$ was found to possess an orthorhombic crystal structure with $Cmc2_1$ space-group symmetry and lattice parameters $a = 3.933$ Å, $b = 26.726$ Å, and $c = 5.683$ Å. Considering that the difference in ionic radii between V^{5+} and Nb^{5+} is small (~15%), V^{5+} is expected to substitute Nb^{5+} in the parent compound $Sr_2Nb_2O_7$ in an isovalent manner.

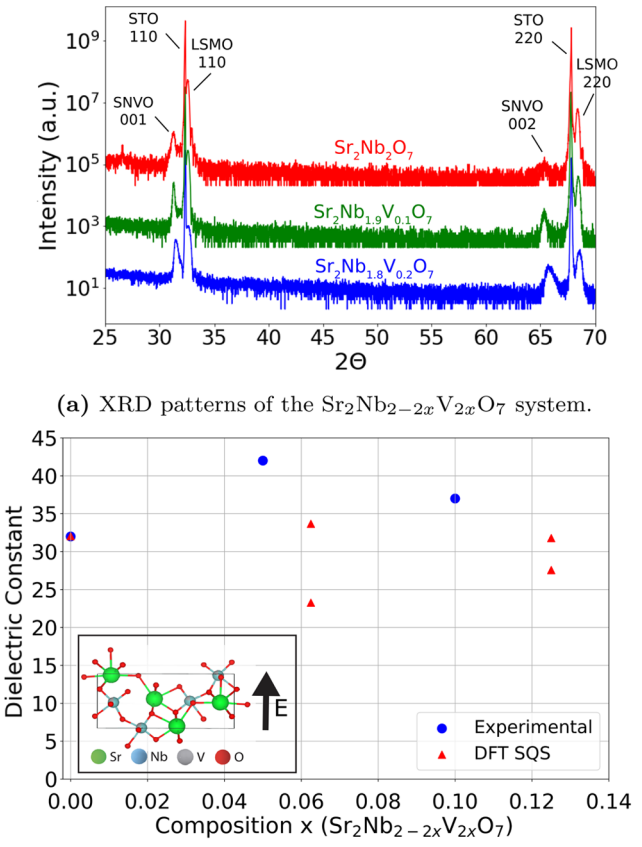

(a) XRD patterns of the $Sr_2Nb_{2-2x}V_{2x}O_7$ system.

(b) Dielectric measurements of the $Sr_2Nb_{2-2x}V_{2x}O_7$ system along the [001] compared to DFT calculations.

Figure 5. $Sr_2Nb_{2-2x}V_{2x}O_7$ alloys were synthesized epitaxially and characterized for crystal structure and dielectric properties.

The structure was found to remain in the crystalline orthorhombic phase as a function of vanadium concentration, as shown in Figure 5a. The thin-film heterostructures for $Sr_2Nb_{2-2x}V_{2x}O_7$ with $x > 0.1$ were found to be challenging to synthesize as a single-phase solid solution due to the film's tendency to decompose to the parent phases: i.e., $Sr_2V_2O_7$ and $Sr_2Nb_2O_7$. Such observations are consistent with prior studies of bulk ceramics and the current study's calculations for a thermodynamically stable solid solution alloy in Figure 3c.[22] In addition to structural characterization, electrical properties of the heterostructures were probed to obtain the dielectric constant of the synthesized compositions. The dielectric constant is measured along [001] and is found to be 32, 42, and 37 for compositions with $x = 0$, 0.05, 0.1 in Figure 5b. Rocking curves, full dielectric measurements, and diffraction data are available as a part of the Supporting Information. We note the enhancement of dielectric constants with vanadium alloying to be promising for the polar properties of this alloy. While DFT results only show a minor increase in dielectric properties with vanadium concentration along [001] compared to experiment, the discrepancy may be due to the epitaxial growth method introducing interfacial strains and the limitations of DFT in modeling large unit cells.

CONCLUSION

Lead-free piezoelectric materials have been the subject of extensive research due to recent global regulations on lead.[2] Computational methods contribute a valuable tool to the high-throughput search for novel materials, especially outside of the traditional perovskite family. However, the exploration of MPBs, which comprise the majority of modern piezoelectric solutions, presents a number of technical challenges for

https://doi.org/10.1021/acs.chemmater.2c00755
Chem. Mater. XXXX, XXX, XXX−XXX

computation. In this study, we first establish the ability of endpoint properties to provide a reasonable qualitative approximation for lattice dynamics in the PZT. We note that the exploration for softened phonon modes in this system correctly implies the presence of the tetragonal to rhombohedral MPB and presents a potential descriptor for high-throughput MPB searches. We then examine the layered perovskite $Sr_2Nb_2O_7$ as a parent compound and employ a Vegard's-law-like approximation for exploring increased polar properties based on the identification of softening phonon modes. A thorough screening of 19 potential cation substitutions for this compound was conducted to search for large piezoelectric response and thermodynamically stable solid solution alloys. From this screening, we identify $Sr_2Nb_{2-2x}V_{2x}O_7$ as a system with predicted enhanced piezoelectric and dielectric properties. We conduct an 88-atom unit cell calculation of the piezoelectric tensor of $Sr_2Nb_{2-2x}V_{2x}O_7$ at x = 0.0625, 0.125 for multiple cation orderings at each composition and find a significant 184% enhanced piezoelectric response of this alloy due to softened phonon modes and a favorable change in the internal strain tensors. Concurrently, slightly enhanced dielectric properties were predicted at the x = 0.0625 composition. Using pulsed-laser deposition, several compositions of the $Sr_2Nb_2O_7$ system were synthesized, which was found to form a solid solution alloy with increased dielectric properties as a function of vanadium doping. We present this material as a candidate for future technological improvements and the screening methodology for the accelerated design of enhanced polar materials, especially with respect to potential MPB systems and high-performing, lead-free piezoelectric materials.

■ ASSOCIATED CONTENT

Supporting Information

The Supporting Information is available free of charge at https://pubs.acs.org/doi/10.1021/acs.chemmater.2c00755.

Additional computational procedures, linear approximation for piezoelectric response alloys of the $Sr_2Nb_2O_7$ system, thermodynamic analysis of alloys of the $Sr_2Nb_2O_7$ system, full PZT linear approximation phonon spectra. (PDF)

Rocking curves, full dielectric measurement data full XRD spectra for 131 and 202 peaks as .csv files (ZIP)

■ AUTHOR INFORMATION

Corresponding Author

Kristin A. Persson − *Material Science and Engineering Department, University of California, Berkeley, California 94704, United States; Materials Sciences Division, Lawrence Berkeley National Laboratory, Berkeley, California 94720, United States; Molecular Foundry, Lawrence Berkeley National Laboratory, Berkeley, California 94720, United States;* orcid.org/0000-0003-2495-5509; Email: kapersson@lbl.gov

Authors

Handong Ling − *Material Science and Engineering Department, University of California, Berkeley, California 94704, United States; Materials Sciences Division, Lawrence Berkeley National Laboratory, Berkeley, California 94720, United States;* orcid.org/0000-0002-7776-9913

Megha Acharya − *Material Science and Engineering Department, University of California, Berkeley, California 94704, United States; Materials Sciences Division, Lawrence Berkeley National Laboratory, Berkeley, California 94720, United States;* orcid.org/0000-0001-9618-1771

Lane W. Martin − *Material Science and Engineering Department, University of California, Berkeley, California 94704, United States; Materials Sciences Division, Lawrence Berkeley National Laboratory, Berkeley, California 94720, United States*

Complete contact information is available at: https://pubs.acs.org/10.1021/acs.chemmater.2c00755

Notes

The authors declare no competing financial interest.

■ ACKNOWLEDGMENTS

This work was primarily supported by the Materials Project, funded by the U.S. Department of Energy, Office of Science, Office of Basic Energy Sciences, Materials Sciences and Engineering Division, under Contract No. DE-AC02-05-CH11231: Materials Project program KC23MP. Computational resources were provided by the National Energy Research Scientific Computing Center, a DOE Office of Science User Facility supported by the Office of Science of the DOE under Contract No. DE-AC02- 05CH11231.

■ REFERENCES

(1) Damjanovic, D. Contributions to the Piezoelectric Effect in Ferroelectric Single Crystals and Ceramics. *J. Am. Ceram. Soc.* **2005**, *88*, 2663.

(2) Bell, A. J.; Deubzer, O. Lead-free piezoelectricsThe environmental and regulatory issues. *MRS Bull.* **2018**, *43*, 581−587.

(3) Lee, H. J.; Zhang, S.; Bar-Cohen, Y.; Sherrit, S. High Temperature, High Power Piezoelectric Composite Transducers. *Sensors (Basel, Switzerland)* **2014**, *14*, 14526−14552.

(4) Panda, P. K.; Sahoo, B. PZT to lead free piezo ceramics: A review. *Ferroelectrics* **2015**, *474*, 128−143.

(5) Zheng, T.; Wu, J.; Xiao, D.; Zhu, J. Recent development in lead-free perovskite piezoelectric bulk materials. *Prog. Mater. Sci.* **2018**, *98*, 552−624.

(6) Armiento, R.; Kozinsky, B.; Fornari, M.; Ceder, G. Screening for high-performance piezoelectrics using high-throughput density functional theory. *Phys. Rev. B* **2011**, *84*, 014103.

(7) Armiento, R.; Kozinsky, B.; Hautier, G.; Fornari, M.; Ceder, G. High-throughput screening of perovskite alloys for piezoelectric performance and thermodynamic stability. *Phys. Rev. B* **2014**, *89*, 134103.

(8) Jiang, X.; Kim, K.; Zhang, S.; Johnson, J.; Salazar, G. High-Temperature Piezoelectric Sensing. *Sensors* **2014**, *14*, 144−169.

(9) de Jong, M.; Chen, W.; Geerlings, H.; Asta, M.; Persson, K. A. A database to enable discovery and design of piezoelectric materials. *Scientific Data* **2015**, *2*, 150053.

(10) Petousis, I.; et al. High-throughput screening of inorganic compounds for the discovery of novel dielectric and optical materials. *Scientific Data* **2017**, *4*, 1−12.

(11) Nakanishi, N.; Nagasawa, A.; Murakami, Y. LATTICE STABILITY AND SOFT MODES. *Journal de Physique Colloques* **1982**, *43*, C4-35−C4-55.

(12) Tomeno, I.; Fernandez-Baca, J. A.; Marty, K. J.; Oka, K.; Tsunoda, Y. Simultaneous softening of acoustic and optical modes in cubic PbTiO 3. *Physical Review B - Condensed Matter and Materials Physics* **2012**, *86*, 134306.

(13) Wang, Y.; Zacherl, C. L.; Shang, S.; Chen, L.-q. Phonon dispersions in random alloys: a method based on special quasi-

random structure force constants. *J. Phys.: Condens. Matter* **2011**, *23*, 485403.
(14) Asta, M. Transferable force-constant modeling of vibrational thermodynamic properties in fcc-based Al−. *Phys. Rev. B* **2007**, *75*, 1−15.
(15) Zhou, F.; Nielson, W.; Xia, Y.; Ozolins, V. Compressive sensing lattice dynamics. I. General formalism *arXiv:1805.08904v3*, 2019, 1−39.
(16) Zhou, F.; Nielson, W.; Xia, Y.; Ozolins, V. Compressive sensing lattice dynamics. I. General formalism*arXiv:1805.08904v3*, 2019, 1−39.
(17) Zhou, F.; Nielson, W.; Xia, Y.; Ozolins, V.Compressive sensing lattice dynamics. I. General formalism *arXiv:1805.08904v3*, 2019, 1−39.
(18) Ling, H.; Dwaraknath, S. S.; Persson, K. A. Origin of Disorder Tolerance in Piezoelectric Materials and Design of Polar Systems. *Chem. Mater.* **2020**, *32*, 2836−2842.
(19) Ning, H.; Yan, H.; Reece, M. J. Piezoelectric Strontium Niobate and Calcium Niobate Ceramics with. *J. Am. Ceram. Soc.* **2010**, *93*, 1409.
(20) Zhang, L.; et al. From Sr2Nb2O7 to CaxSr2-xNb2O7: An Effective Enhancement of Nonlinear Optical Activity by a Simple Way of Cation Substituting. *Cryst. Growth Des.* **2018**, *18*, 4140−4149.
(21) Gao, Z.; et al. The Effect of Barium Substitution on the Ferroelectric Properties of Sr 2 Nb 2 O 7 Ceramics. *J. Am. Ceram. Soc.* **2013**, *96*, 1163−1170.
(22) Seraji, S.; et al. Processing and properties of vanadium doped strontium niobate. *Materials Science and Engineering: B* **2002**, *88*, 73−78.
(23) Honda, A.; Shi-chang, L.; Yuan-lei, Z. First principles study on lattice vibration and electrical properties of layered perovskite Sr 2 × 2 O 7 (x = Nb, Ta). *Chinese Physics B* **2018**, *27*, 086104.
(24) Baroni, S.; Teorica, F.; Trieste, U.; Giannozzi, P.; Testa, A. Green's-Function Approach to Linear Response in Solids Stefano. *Phys. Rev. Lett.* **1987**, *58*, 1861−1864.
(25) Baroni, S.; et al. Phonons and related crystal properties from density-functional perturbation theory. *REVIEWS OF MODERN PHYSICS* **2001**, *73*, 515.
(26) Gonze, X. Adiabatic density-functional perturbation theory. *Phys. Rev. A* **1995**, *52*, 1096.
(27) Kresse, G.; Hafner, J. Ab initio molecular dynamcis for liquid metals. *Phys. Rev. B* **1993**, *47*, 558−561.
(28) Kresse, G.; Furthmu, J. Efficient iterative schemes for ab initio total-energy calculations using a plane-wave basis set. *PHYSICAL REVIEW B* **1996**, *54*, 11169.
(29) Perdew, J. P.; Burke, K.; Ernzerhof, M. Generalized Gradient Approximation Made Simple John. *Phys. Rev. Lett.* **1996**, *77*, 3865−3868.
(30) Wu, X.; Vanderbilt, D.; Hamann, D. R. Systematic treatment of displacements, strains, and electric fields in density-functional perturbation theory. *Physical Review B - Condensed Matter and Materials Physics* **2005**, *72*, 1.
(31) Körmann, F.; Yuji, I.; Blazej, G.; Marcel, S. Phonon broadening in high entropy alloys. *npj Computational Materials* **2017**, *3*, 1−8.
(32) Aykol, M.; Dwaraknath, S. S.; Sun, W.; Persson, K. A. Thermodynamic limit for synthesis of metastable inorganic materials. *Science Advances* **2018**, *4*, 1−8.
(33) Togo, A.; Tanaka, I. First principles phonon calculations in materials science. *Scripta Materialia* **2015**, *108*, 1−5.
(34) van de Walle, A.; Asta, M.; Ceder, G. The alloy theoretic automated toolkit: A user guide. *Calphad* **2002**, *26*, 539−553.
(35) Jaffe, H.; Berlincourt, D. A. Piezoelectric transducer materials. *Proceedings of the IEEE* **1965**, *53*, 1372−1386.
(36) Energy above the hull refers to the energy of decomposition of a material into the most stable compounds at a specific composition.

https://doi.org/10.1021/acs.chemmater.2c00755
Chem. Mater. XXXX, XXX, XXX−XXX